Theory of symmetry-resolved quench-drive spectroscopy: Nonlinear response of phase-fluctuating superconductors

Matteo Puviani ⊙*

Max Planck Institute for the Science of Light, 91058 Erlangen, Germany

Recent experiments on cuprates have shown the possibility of opening a gap above the superconducting critical temperature, in the so-called phase-fluctuating state, by enhancing the phase coherence of preformed Cooper pairs. Quench-drive spectroscopy, an implementation of 2D coherent spectroscopy, has emerged as a powerful tool for investigating out-of-equilibrium superconductors and their collective modes. In this paper, we enrich the quench-drive scheme by developing a systematic generalization to study the nonlinear response of *d*-wave incoherent Cooper pairs in a symmetry-resolved manner. In particular, we not only show that it is possible to obtain a third-harmonic signal from fully incoherent pairs with an equilibrium vanishing order parameter, but we also characterize the full flourishing 2D spectrum of the generated nonlinear response. The results provide a deeper theoretical insight on recent experimental results, opening the door to a symmetry-driven design of future experiments on unconventional and enhanced superconductors.

I. INTRODUCTION

Since their discovery, high-temperature superconductors have been intensely studied because of their properties and rich phase diagram [1–3]. These unconventional superconductors are characterized by a complex order parameter whose value depends on the quasiparticles' crystal momentum: it can assume both positive and negative values with maximum absolute value at the antinodal points of the Brillouin zone, while vanishing at the nodal points [4]. This character is a result of the B_{1g} symmetry of the $d_{x^2-y^2}$ superconducting pairing, descending from their D_{4h} crystal structure [5,6]. However, some features of this class of materials are still under debate, such as the conditions and possibility to induce and experimentally observe collective modes [7–14] or the origin of the pseudogap phase [15–17].

In particular, various attempts have been made to study and detect the amplitude Higgs mode even in unconventional superconductors, both investigating the nonequilibrium nonlinear behavior of these materials [12,18] and characterizing the symmetries of their response [19,20]. Recent advances have shown that the nonlinear behavior of unconventional superconductors when probed by light emerges as the blending of different contributions, depending on electron-hole doping and impurity concentration, among others [21–23].

Beside this, it has been suggested that the pseudogap phase is a precursor of the superconducting state, characterized by finite pairing strength and preformed Cooper pairs with phase incoherence [15,16,24]. Even if this picture is controversial and has been disproved to some extent, in cuprates, in a region of the phase diagram above the superconducting critical temperature, the superconducting phase is incoherent [25–27].

When an electromagnetic field interacts with a phase-fluctuating superconductor, for some values of intensity and frequency of the incident radiation, it is possible to induce phase coherence among preexisting phase-incoherent Cooper pairs: this process is responsible for the transient enhancement of the order parameter or the appearance of a finite superconducting gap in the case of complete phase-incoherence [24,28]. If this transition from an incoherent to a partially coherent phase is fast enough, such as when induced by a short-time quench pulse, then oscillations of the order parameter (quasiparticles' and amplitude mode's excitations) can be produced as well, similarly to what happens in light-induced superconductors [29].

Moreover, the generation of odd higher harmonics from driven superconductors has been theoretically shown and experimentally observed: this result originates from the nonlinear behavior of the optical kernel in the superconducting state [8,18]. 2D coherent spectroscopy (2DCS) on superconductors [30] has developed as a systematic generalization of pump probe [31] in the context of the broader concept of high-dimensional spectroscopy [32–36]. In addition, quench-drive spectroscopy [Fig. 1(a)] has been proposed by Puviani *et al.* [37,38] as a specific scenario of THz 2DCS to study superconductors, combining a few-cycle short-time quench pulse and a long-time multicycle driving field. This allows us to obtain a complex 2D nonlinear response embedding many nonlinear contributions, providing useful information on the
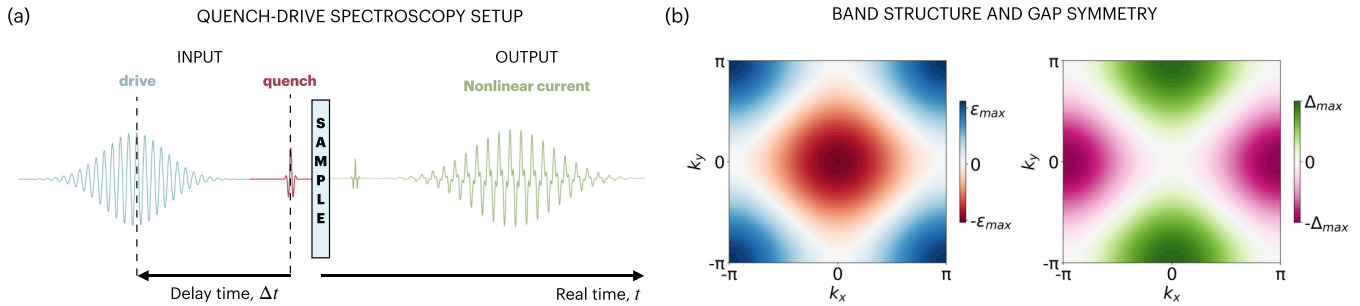
---

*Contact author: matteo.puviani@mpl.mpg.de

FIG. 1. Quench-drive spectroscopy of unconventional superconductors. (a) The 2D quench-drive spectroscopy is performed with a short (quench) pulse, followed by a long Gaussian-shaped (drive) pulse at a delayed time Δt. The output signal is analyzed as a function of the real time t. (b) Band structure (on the left) and $d_{x^2-y^2}$ gap symmetry (on the right) of the unconventional superconductors studied in this paper. The nodal points are identified with $\Delta_{\mathbf{k}} = 0$, for $\mathbf{k} = (k_x, k_y = \pm k_x)$, while the antinodal ones are at $\mathbf{k} = (0, \pm\pi), (\pm\pi, 0)$.

optical kernel of the superconductor. In fact, this technique can be used on superconductors to study high-harmonic generation and to address quasiparticles' excitations as well as collective states, as shown by a recent experimental realization [39]. Since then, these two-dimensional spectroscopies have been widely developed [40–43], proving to be suitable for extracting information and details on the superconducting order parameter and its collective modes [23,44].

In this paper, we combine the quench-drive spectroscopy technique, which allows us to investigate the nonequilibrium behavior of materials, with the symmetry selection allowed by pulses' polarization typically used in other spectroscopic techniques, such as Raman [5,45,46] or birefringence [28] spectroscopy. Here, we study the nonlinear response to quench drive pulses of fully phase-incoherent Cooper pairs with $d_{x^2-y^2}$-wave pairing symmetry [Figs. 1(b) and 1(c)], as in unconventional superconductors. In particular, we systematically investigate the order parameter's dynamics and the high-harmonic generation process as a function of the real time and quench-drive delay time, as well as their Fourier spectra. The main results of our paper can be summarized with the following points:

(1) The presence of nonlinear response even with vanishing order parameter at equilibrium.

(2) The induced gap oscillations have predominant B_{1g} and B_{2g} symmetry according to the spectroscopy scheme.

(3) The nonlinear current response has B_{1g} or B_{2g} symmetry according to whether it originates from the driving or the quench pulse, respectively.

(4) The third-harmonic generation originates from predominant B_{1g} symmetry excitation.

We also want to highlight that all these results are directly experimentally accessible, and the first one suggests that our approach can be used for testing the hypothesis of incoherent pairs above T_c. In addition, while the first result does not necessarily require a symmetry-resolved quench-drive spectroscopy scheme to be obtained (even if only partial information would otherwise be caught), the other results are only achievable with the use of the symmetry-resolved technique introduced in this paper.

The paper is organized as follows: In Sec. II, we provide a brief theoretical overview of nonlinear current generation by incoherent Cooper pairs with $d_{x^2-y^2}$ symmetry. In Sec. III, we describe the foundations of symmetry-resolved quench-drive

spectroscopy. In Sec. IV, we show and analyze the numerical results, studying the symmetry-resolved nonlinear response obtained for different configurations of quench and drive pulses. Eventually, in Sec. V we conclude summarizing the paper and providing an outlook for possible extensions and future research. In Appendices A and B, we propose the full theoretical calculations of the pseudospin model and the quench-drive nonlinear response generation, while in Appendix C we provide more results, obtained with a different choice of the quench and drive frequencies.

II. NONLINEAR RESPONSE OF INCOHERENT COOPER PAIRS

In this section, we theoretically investigate the nonlinear current generated by a material in a state with phase-fluctuating superconductivity subject to quench and drive pulses. The result is obtained by solving the Bloch equations derived from the pseudospin model of the BCS Hamiltonian described in Appendices A and B.

In cuprates, recent experimental results have shown the presence of superconducting fluctuations even above the superconducting critical temperature [47]. This behavior has been explained by postulating the presence of incoherent Cooper pairs: in this picture, while the pairing persists even above the critical superconducting temperature, the Cooper pairs lose their phase coherence [48]. This has been experimentally supported by further photoemission [49], magnetization [50], and transport measurements [51,52], which suggest the presence of local correlations and superconducting pairing above the critical temperature [24]. Therefore, to model the state with phase-fluctuating superconductivity characterized by the presence of preformed incoherent pairs, we consider an artificial equilibrium superconducting state obtained by adding a random momentum-dependent phase $\phi_{\mathbf{k}}$ to the original Cooper pairs' state, as in Ref. [28]. As a result, the strength of the pairing potential remains unchanged, as well as the number of total Cooper pairs, while the superconducting order parameter decreases due to the reduced coherence. According to the maximum angle $\phi_{\max}$ which defines the range of the random phase $\phi_{\mathbf{k}}$, with $\phi_{\mathbf{k}} \in [-\phi_{\max}, +\phi_{\max}]$ we are able to describe different conditions of the material from the pure superconducting phase for $\phi_{\max} = 0$ to the complete loss of coherence for $\phi_{\max} = \pi$.

We define the gap of the pure superconducting state $\Delta_{\mathbf{k}}^{(0)} = \Delta_0^{(0)} f_{\mathbf{k}}$ and the superconducting order parameter in the presence of incoherent pairs as $\tilde{\Delta}_{\mathbf{k}}^{(\phi)} = \tilde{\Delta}^{(\phi)} f_{\mathbf{k}}$, such that

$$\tilde{\Delta}^{(\phi)} = V \sum_{\mathbf{k}'} f_{\mathbf{k}'}^2 \frac{\Delta_0^{(0)}}{2E_{\mathbf{k}'}^{(0)}} e^{i\phi_{\mathbf{k}'}}, \tag{1}$$

where V is the same pairing strength of the original state, and $E_{\mathbf{k}}^{(0)} = \sqrt{\epsilon_{\mathbf{k}}^2 + (\Delta_{\mathbf{k}}^{(0)})^2}$. We notice that the order parameter is calculated with the sum of the coherent contributions over all the Cooper pairs in momentum space. In phase-fluctuating superconductors, the global coherence is lost as the Cooper pairs acquire an additional momentum-dependent phase ϕ_k. The superconducting gap in the new equilibrium state can be written in the pseudospin formalism as [53]

$$\tilde{\Delta}_{\mathbf{k}}^{(\phi)} = V f_{\mathbf{k}} \sum_{\mathbf{k}'} f_{\mathbf{k}'}(\tilde{\sigma}_{\mathbf{k}',x} - i\tilde{\sigma}_{\mathbf{k}',y}), \tag{2}$$

where $f_{\mathbf{k}}$ is the $d_{x^2-y^2}$-wave symmetry of the superconducting pairing. Moreover, we have introduced the equilibrium pseudospin components:

$$\tilde{\sigma}_{\mathbf{k},x} = \sigma_{\mathbf{k},x} \cos \phi_{\mathbf{k}} = f_{\mathbf{k}} \frac{\Delta_0^{(0)} \cos \phi_{\mathbf{k}}}{2E_{\mathbf{k}}^{(0)}}$$

$$\tilde{\sigma}_{\mathbf{k},y} = -\sigma_{\mathbf{k},x} \sin \phi_{\mathbf{k}} = -f_{\mathbf{k}} \frac{\Delta_0^{(0)} \sin \phi_{\mathbf{k}}}{2E_{\mathbf{k}}^{(0)}}$$

$$\hat{\tilde{\sigma}}_{\mathbf{k}}^z = \hat{\sigma}_{\mathbf{k}}^z. \tag{3}$$

To describe the dynamics of the system, we use the Heisenberg's equation of motion

$$\partial_t \tilde{\sigma}_{\mathbf{k}} = \tilde{\mathbf{b}} \times \tilde{\sigma}_{\mathbf{k}}, \tag{4}$$

with the new pseudomagnetic field defined as

$$\tilde{\mathbf{b}} = (-2\tilde{\Delta}' f_{\mathbf{k}}, -2\tilde{\Delta}'' f_{\mathbf{k}}, 2\epsilon_{\mathbf{k}}). \tag{5}$$

In the presence of an external gauge field represented by the vector potential $\mathbf{A}(t)$ coupling to the electrons, the pseudospin changes in time according to

$$\tilde{\sigma}_{\mathbf{k}}(t) = \tilde{\sigma}_{\mathbf{k}}(0) + \delta\tilde{\sigma}_{\mathbf{k}}(t). \tag{6}$$

The vector potential is not restricted here to any particular form, but in the context of quench-drive spectroscopy we will describe is as the sum of the quench and drive pulses' contributions, $\mathbf{A}(t) = \mathbf{A}_q(t) + \mathbf{A}_d(t) = \overline{\mathbf{A}}_q(t - t_q) + \overline{\mathbf{A}}_d(t - t_d)$. Here $\mathbf{A}_{q(d)}(t)$ is the vector potential of the quench (drive) pulse only, with amplitude $A_{q(d)}$, respectively, while $\overline{\mathbf{A}}_{q(d)}$ is the quench (drive) pulse shape, shifted at center time $t_{q(d)}$, respectively. The external electromagnetic field is included in the pseudomagnetic field by means of the Peierls' minimal substitution $\mathbf{k} \rightarrow \mathbf{k} - e\mathbf{A}(t)$ in the fermionic energy, resulting in

$$\tilde{\mathbf{b}}_{\mathbf{k}}(t) = (-2\tilde{\Delta}'(t) f_{\mathbf{k}}, -2\tilde{\Delta}''(t) f_{\mathbf{k}}, \varepsilon_{\mathbf{k}-e\mathbf{A}(t)} + \varepsilon_{\mathbf{k}+e\mathbf{A}(t)}). \tag{7}$$

Here we considered the limit of a small superconducting gap velocity (in comparison to the electron velocity), so the minimal coupling of the pairing term can be neglected [54]. The equation of motion in Eq. (4) can be decomposed into a set of differential equations, whose solution provides the

time-dependent value of the pseudospin $\tilde{\sigma}_{\mathbf{k}}(t)$. Once this term is known, we can obtain the value of the time-dependent order parameter $\tilde{\Delta}^{(\phi)}(t) = \tilde{\Delta}^{(\phi)}(0) + \delta\tilde{\Delta}^{(\phi)}(t)$, as well as the generated nonlinear current (see Appendix B). However, we notice that the complex order parameter can be written as

$$\tilde{\Delta}^{(\phi)} = |\tilde{\Delta}^{(\phi)}| \, e^{i\theta}, \tag{8}$$

where θ is the global phase of the superconducting gap. However, an additional momentum-dependent phase appears in the definition of the order parameter according to Eq. (1): as a result, the gap equation is not self-consistent anymore and the value of the gap is subject to some time-dependent noise due to the phase incoherence of the preformed pairs.

In the full generated current, we can distinguish two non-vanishing contributions, namely, a linear component with the same oscillating behavior of the driving field $\mathbf{A}(t)$,

$$\mathbf{j}^{(1)}(t) = -e^2 \sum_{\mathbf{k}} \mathbf{A}(t) \cdot \nabla_{\mathbf{k}} \mathbf{v}_{\mathbf{k}} \left(2\hat{\tilde{\sigma}}_{\mathbf{k}}^z(0) + 1\right), \tag{9}$$

and a nonlinear term including all higher orders:

$$\mathbf{j}^{(NL)}(t) = e \sum_{\mathbf{k}} \mathbf{v}_{\mathbf{k}-e\mathbf{A}(t)} \left(2\hat{\tilde{\sigma}}_{\mathbf{k}}^z(t) - 2\hat{\tilde{\sigma}}_{\mathbf{k}}^z(0)\right). \tag{10}$$

Since the third pseudospin component in equilibrium is independent on the phase coherence [Eq. (3)], the linear current in Eq. (9) is always nonzero, even for fully incoherent Cooper pairs and vanishing gap.

More details on the solution of the equation of motion and the derivation of the generated current for the quench-drive setup are provided in Appendices A and B.

III. SYMMETRY-RESOLVED NONLINEAR 2D SPECTROSCOPY

In this section, we propose the theoretical foundations for the symmetry-resolved quench-drive spectroscopy, identifying the main nonlinear components for different configurations and their corresponding symmetry [55].

First, we can conveniently write the frequency spectrum of gap oscillations, as obtained from the solution of the Bloch equations after transforming into Fourier space, with (ω, ν) as the conjugate of the time variables $(t, \Delta t)$, using the convolution operation $(*)$ defined as $[B * C](x) = \int dy \, B(y) C(x - y)$ [38].

$$\delta\Delta_{\mathbf{k}}(\omega, \nu) \propto [A_i * A_j](\omega, \nu) \, \gamma_{ij}(\mathbf{k}), \tag{11}$$

with $i, j \in \{x, y\}$ and the vector potential $A_{i,j}$ including both the quench and the driving fields. The Raman-like factor $\gamma_{ij}(\mathbf{k}) = \nabla_{\mathbf{k}}(\mathbf{v}_{\mathbf{k}} \cdot \hat{j})$ (where $\hat{j}$ is the unitary vector along the direction of j) represents the second-order light-matter coupling and includes the overall symmetry of the gap oscillations (Fig. 2). In this paper, we are considering unconventional superconductors characterized by a D_{4h} crystal symmetry, with $d_{x^2-y^2}$ order parameter. For this point-group symmetry, the only relevant irreducible representations (irreps) are A_{1g}, B_{1g} and B_{2g}. Therefore, the Raman-like factors can be decomposed into the irreps of the D_{4h} point group as follows [45]:

$$\gamma_{xx} = \gamma_{A_{1g}} + \gamma_{B_{1g}}, \tag{12a}$$

$$\gamma_{yy} = \gamma_{A_{1g}} - \gamma_{B_{1g}}, \tag{12b}$$

FIG. 2. Table of symmetries of Raman factors, γ_{rs}, with $r, s \in \{q, p\}$, where the labels q and p represent the quench and drive pulses' directions, respectively.

$$\gamma_{xy} = \gamma_{B_{2g}}, \tag{12c}$$

$$\gamma_{x'x'} = \gamma_{A_{1g}} + \gamma_{B_{2g}}, \tag{12d}$$

$$\gamma_{x'y'} = \gamma_{B_{1g}}, \tag{12e}$$

$$\gamma_{y'y'} = \gamma_{A_{1g}} - \gamma_{B_{2g}}, \tag{12f}$$

$$\gamma_{x'x} = (\gamma_{A_{1g}} + \gamma_{B_{1g}} + \gamma_{B_{2g}})/\sqrt{2}, \tag{12g}$$

$$\gamma_{x'y} = (\gamma_{A_{1g}} - \gamma_{B_{1g}} + \gamma_{B_{2g}})/\sqrt{2}, \tag{12h}$$

with $\hat{x}' = (\hat{x} + \hat{y})/\sqrt{2}$ and $\hat{y}' = (\hat{x} - \hat{y})/\sqrt{2}$, corresponding to an angle with respect to the $\hat{x}$ axis of $\pi/4$ and $-\pi/4$, respectively. The general rule given the angles α and θ with respect to the $\hat{x}$ axis reads [28]

$$\gamma_{\alpha\theta}(\mathbf{k}) = \gamma_{A_{1g}} \cos(\alpha - \theta) + \gamma_{B_{1g}} \cos(\alpha + \theta)$$
$$+ \gamma_{B_{2g}} \sin(\alpha + \theta). \tag{13}$$

Similarly, the third-order nonlinear current, which represents the lowest-order nonvanishing nonlinear contribution, can be written as

$$j_i^{(3)}(t, \Delta t) \propto A_j(t, \Delta t) \sum_{\mathbf{k}} \gamma_{ij}(\mathbf{k}) \, \delta\tilde{\sigma}_{\mathbf{k}}^z(t, \Delta t), \tag{14}$$

with $i, j, k, l \in \{x, y\}$. We notice that in this expression the order parameter's oscillations of Eq. (11) are embedded into the time-dependent pseudospin component $\delta\tilde{\sigma}_{\mathbf{k}}^z(t, \Delta t)$. It is convenient to consider its spectrum in Fourier space, where (ω, ν) are the conjugate of the variables $(t, \Delta t)$, as

$$j_i^{(3)}(\omega, \nu) \propto \sum_{j,k,l} \int d\omega_1 d\omega_2 d\omega_3 \, \chi_{ijkl}^{(3)}(\omega - \omega_1) \, A_j(\omega_1)$$
$$\times A_k(\omega_2) A_l(\omega_3) \, \delta(\omega - \omega_1 - \omega_2 - \omega_3), \tag{15}$$

where the delta function over the frequencies enforces energy conservation. Here we also introduced the third-order nonlinear susceptibility $\chi_{ijkl}^{(3)} = \gamma_{ij} \, \gamma_{kl} \, \chi_{\rho\rho}^{(3)}$, where $\chi_{\rho\rho}^{(3)}$ is the third-order density-density response function. Here we omitted the sum over $\mathbf{k}$ and the frequency dependencies for convenience of notation.

As an example, we can derive the symmetry of the $xyx'y$ response, which enters the nonlinear current along the x direction with interaction of pulses along $\hat{x}'$ and $\hat{y}$ as follows:

$$\chi_{xyx'y}^{(3)} = \chi_{\rho\rho}^{(3)} \, \gamma_{xy} \, \gamma_{x'y}$$
$$= \chi_{\rho\rho}^{(3)} \, \gamma_{B_{2g}} (\gamma_{A_{1g}} - \gamma_{B_{1g}} + \gamma_{B_{2g}})/\sqrt{2} = \chi_{B_{2g}}^{(3)}/\sqrt{2}, \tag{16}$$

with $\chi_{B_{2g}}^{(3)} = \chi_{\rho\rho}^{(3)} \, \gamma_{B_{2g}} \, \gamma_{B_{2g}}/\sqrt{2}$, which is the only nonvanishing term in Eq. (16) after summing over the full Brillouin zone. When analyzing the quench-drive spectra, we can substitute the subscripts m, q, and d representing the measurement, quench and drive *axis*, respectively, to Eqs. (11), (14), and (15).

As shown by Puviani et al. [38], there are six contributions of the third-order nonlinear susceptibility in a quench-drive spectroscopy setup, which sum up to provide the full nonlinear response, namely (Fig. 3),

$$\chi^{(3)} = \chi_{mddd}^{(3)} + \chi_{mddq}^{(3)} + \chi_{mqdd}^{(3)}$$
$$+ \chi_{mdqq}^{(3)} + \chi_{mqqd}^{(3)} + \chi_{mqqq}^{(3)}. \tag{17}$$

Each of them can be decomposed into the D_{4h} symmetry *irreps* as shown before. For example, selecting the output along the x axis parallel to the driving field, and with a quench pulse along the $\hat{x}y$ diagonal, i.e., $m = x$, $q = x'$, $d = x$, for the purely driving response, we get

$$\chi_{mddd}^{(3)} = \chi_{\rho\rho}^{(3)} \, \gamma_{md} \, \gamma_{dd}$$
$$= \chi_{A_{1g}}^{(3)} + \chi_{B_{1g}}^{(3)}, \tag{18}$$

where the first Raman factor represents the measurement-driving vertex, while the second corresponds to the driving-driving one. Analogously, for the mixed quench-drive response quadratic in the quench amplitude field, we have

$$\chi_{mdqq}^{(3)} = \chi_{\rho\rho}^{(3)} \, \gamma_{md} \, \gamma_{qq} = \chi_{A_{1g}}^{(3)} \tag{19}$$

and

$$\chi_{mqqd}^{(3)} = \chi_{\rho\rho}^{(3)} \, \gamma_{mq} \, \gamma_{qd}$$
$$= (\chi_{A_{1g}}^{(3)} + \chi_{B_{1g}}^{(3)} + \chi_{B_{2g}}^{(3)})/\sqrt{2}, \tag{20}$$

which will appear at $\nu \neq 0$ in the two-dimensional quench-drive Fourier spectrum of the nonlinear response.

Interestingly, this example shows in practice how the nature of the two-dimensional spectroscopy allows us to extract an A_{1g} symmetry response (and, similarly, the B_{1g} and B_{2g}) from only one susceptibility component. Moreover, the presence of multiple contributions for different values of the 2D frequency components (ω, ν) allows us to measure and selectively address all the symmetries response with only one experiment.

IV. NUMERICAL RESULTS AND DISCUSSION

In this section, we present the results obtained from the numerical implementation of the expressions and time-dependent Bloch equations show in Secs. II and III. We modeled the electronic band dispersion of the unconventional superconductor as $\epsilon_{\mathbf{k}} = -2t(\cos k_x + \cos k_y) - \mu$, where the quasimomentum components are expressed in units of the lattice constant a. We used the values of $t = 125$ meV for the nearest-neighbor hopping energy, chemical potential $\mu/t = -0.2$, obtaining an electron occupation $n = 0.9$ as in Ref. [24]. For the $d_{x^2-y^2}$ order parameter $\Delta_{\mathbf{k}}^{(0)} = \Delta_{\max}^{(0)}(\cos k_x - \cos k_y)/2$, we chose the value $\Delta_{\max}^{(0)} = 31$ meV. The calculations were performed with a summation over the full Brillouin zone $\{k_x, k_y\} \in \{-\pi, \pi\}$ with a homogeneous
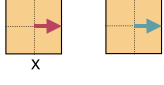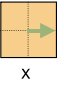
NONLINEAR TERMS

	$\chi^{(3)}_{mddd}$	$\chi^{(3)}_{mddq}$	$\chi^{(3)}_{mqdd}$	$\chi^{(3)}_{mdqq}$	$\chi^{(3)}_{mqqd}$	$\chi^{(3)}_{mqqq}$	
(I) (a)	$A_{1g} + B_{1g}$	$A_{1g} + B_{1g}$	$A_{1g} + B_{1g}$	$A_{1g} + B_{1g}$	$A_{1g} + B_{1g}$	$A_{1g} + B_{1g}$	(a)
(I) (b)	0	0	0	0	0	0	(b)
(II) (a)	$(A_{1g} + B_{2g})/\sqrt{2}$	$(A_{1g} + B_{2g})/\sqrt{2}$	$(A_{1g} + B_{2g})/\sqrt{2}$	$(A_{1g} + B_{2g})/\sqrt{2}$	$(A_{1g} + B_{2g})/\sqrt{2}$	$(A_{1g} + B_{2g})/\sqrt{2}$	(a)
(II) (b)	$(A_{1g} + B_{2g})/\sqrt{2}$	$(A_{1g} + B_{2g})/\sqrt{2}$	$(A_{1g} + B_{2g})/\sqrt{2}$	$(A_{1g} + B_{2g})/\sqrt{2}$	$(A_{1g} + B_{2g})/\sqrt{2}$	$(A_{1g} + B_{2g})/\sqrt{2}$	(b)
(III) (a)	$A_{1g} + B_{1g}$	$(A_{1g} + B_{1g})/\sqrt{2}$	$(A_{1g} + B_{1g})/\sqrt{2}$	A_{1g}	$(A_{1g} + B_{1g} + B_{2g})/\sqrt{2}$	$(A_{1g} + B_{2g})/\sqrt{2}$	(a)
(III) (b)	0	$B_{2g}/\sqrt{2}$	$(A_{1g} - B_{1g})/\sqrt{2}$	B_{2g}	$(A_{1g} - B_{1g} + B_{2g})/\sqrt{2}$	$(A_{1g} + B_{2g})/\sqrt{2}$	(b)

FIG. 3. Table of symmetry-resolved nonlinear spectra contributions. The table shows the six symmetry-resolved components of the third-order nonlinear susceptibility $\chi^{(3)}_{ijkl} \propto \chi^{(3)}_{\rho\rho}\gamma_{ij}\gamma_{kl}$ (with $\{i, j, k, l\} \in \{m, q, d\}$), which are the measurement, quench and drive axis, respectively) in a 2D quench-drive spectrum on a D_{4h} crystal. We considered three (I)–(III) given input (quench and drive) directions as well as two (a), (b) measurement axes.

square sampling and a total number of k points $N_\mathbf{k} = 10^6$. For the time-dependent evolution, we used a time step of $\delta t = 3 \times 10^{-4}$ ps, and for the quench-drive delay $\delta\Delta t = 2.5 \times 10^{-2}$ ps. For the pulses, we used a few-cycle quench and a Gaussian-shaped long-duration drive, with vector field amplitudes for the quench and drive pulses $A_q = 0.8$ and $A_d = 0.8$, respectively. Both of the pulses have been described by sinusoidal functions with frequencies Ω_q and Ω_d, respectively, and Gaussian envelopes of shape $e^{-(t-t_{q,d})/(2\sigma_{q,d}^2)}$ with $2\sigma_q^2 = 0.01$ ps^2 and $2\sigma_d^2 = 5$ ps^2, respectively. Moreover, we set the reference time $t = 0$ at the center of the Gaussian envelope of the driving pulse. The maximum intensity used for each pulse is provided for the corresponding vector potential in units of $\hbar/(e\,a)$, where e is the electron charge and a the lattice constant. Moreover, we chose the frequency of quench (Ω_q) and drive (Ω_d) to be different but both in the THz spectrum, with values $\Omega_d = 11$ THz and $\Omega_q = 7$ THz. In general, different choices of amplitude and frequencies can be made to suppress or enhance specific symmetry contributions. In this paper, we focused on the fully phase-incoherent Cooper pairs, with $\phi_{\max} = \pi$, for which $\tilde{\Delta}^{(\phi)} = 0$.

In our calculations and analysis, we restricted ourselves to only three quench-drive symmetry configurations. These can be addressed in terms of the quench and drive angles defined with respect to the $\hat{x}$ axis α_q and α_d, respectively, as follows:

$$(I) \quad \alpha_q = 0 \quad \alpha_d = 0, \tag{21a}$$

$$(II) \quad \alpha_q = \pi/4 \quad \alpha_d = \pi/4, \tag{21b}$$

$$(III) \quad \alpha_q = \pi/4 \quad \alpha_d = 0. \tag{21c}$$

We studied the behavior of the superconducting gap (Sec. IV A) and the generated nonlinear current (Sec. IV B)

along the (a) x and (b) y direction, as well as their corresponding 2D spectra.

More results, obtained with drive and quench frequencies $\Omega_d = 3.66$ THz and $\Omega_q = 7.48$ THz, respectively, are provided in Appendix C: in this case, the quench pulse is nearly resonant with the bare superconducting gap, while the drive is at a much lower energy.

A. Emergent superconducting gap and oscillations

First, we calculated the behavior of the order parameter, i.e., the superconducting gap, within the quench-drive spectroscopy setup. In Figs. 4(a)(I)–4(a)(III), we show the 2D time-dependent behavior of the absolute value of the gap. In all our simulations, we have set the reference time $t = 0$ at the center of the Gaussian envelope of the driving pulse. Since the initial system is formed by incoherent pairs, the initial superconducting gap is zero. However, when the quench and drive pulses perturb the incoherent state, they are able to induce coherence in the Cooper pairs, giving rise to a finite gap value, in accordance with Ref. [28]. However, thanks to the quench-drive spectroscopic technique, exploiting the symmetry resolution for different quench and drive directions, we can analyze more in depth the gap behavior and the symmetry of its oscillations. Indeed, in Ref. [24] it was shown that a quench pulse along the x axis, i.e., with $\alpha_q = 0$, tends to reduce the superconducting gap decreasing coherence, while with $\alpha_q = \pi/4$ it is increased. Here, we go beyond that scheme, observing that, with the given frequencies of the pulses, a long driving pulse with $\alpha_d = 0$ can also induce coherence in a fully incoherent setup, while a quench along the same direction keeps suppressing it [Figs. 4(a)(I) and 4(a)(III)]. On the other hand, a long driving pulse with $\alpha_d = \pi/4$ can also increase
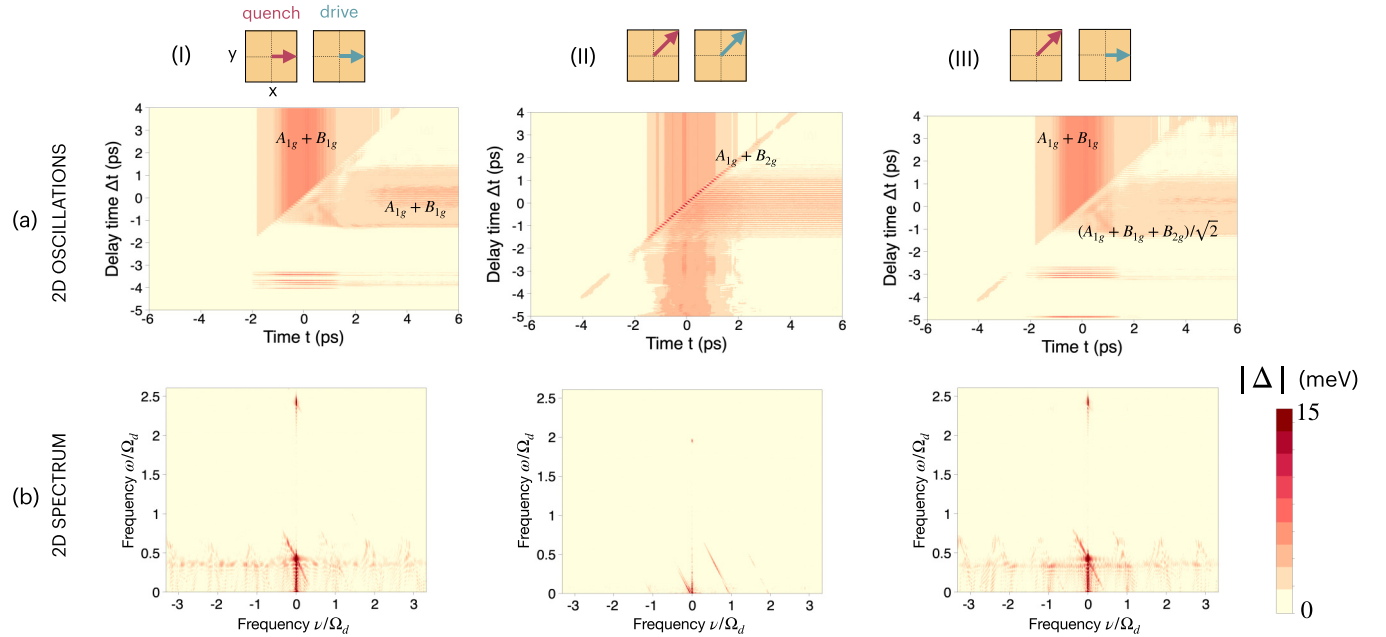
FIG. 4. Gap oscillations and frequency spectra. (a) 2D oscillations in $(t, \Delta t)$ of the absolute value of the superconducting gap, $|\Delta|$, for the three scheme configurations (I)–(III) described in the main text and illustrated by the plots of quench and drive pulses. The main symmetry contributions are written for the strongest signals, according to the table in Fig. 2. (b) Absolute value of the 2D Fourier transform of the full complex gap, $|\mathcal{F}\{\Delta(t, \Delta t)\}| = |\Delta(\omega, \nu)|$.

the gap coherence, but with less efficiency [Fig. 4(a)(II)]. To understand this, we can use the symmetry table in Fig. 2: in fact, for both Figs. 4(a)(I) and 4(a)(III) conditions, the pairs are excited mainly in the B_{1g} symmetry channel. On the contrary, in the Fig. 4(a)(II) scheme, the gap is excited with a predominant B_{2g} symmetry. As a consequence, the B_{1g} symmetry enhances the gap if used in a driving, while it tends to suppress it if imposed by a short quench.

Additional information can be extracted from the analysis of the 2D Fourier spectra of the complex gap, as shown in Fig. 4(b). On the one hand, there is a $2\Omega_d$ oscillation for the (II) scheme, which results from the B_{2g} excitation, while no 2Δ peak (originating from quasiparticles' and amplitude mode excitations) appears here. On the other hand, in schemes (I) and (III), where the B_{1g} symmetry is mainly excited as the relevant one, we notice dominant frequency components at $\omega \approx 0.5 \, \Omega_d$ and $\omega \approx 2.5 \, \Omega_d$. The reason is that within this symmetry the dominant excitation of the superconducting gap is provided by the quasiparticles' excitation and amplitude mode, which have an intrinsic frequency of $\omega = 2\tilde{\Delta}^{(\phi)}$ and $\omega \approx 0.4 \, \tilde{\Delta}^{(\phi)}$, as predicted in Ref. [20].

B. Nonlinear current generation

Since the order parameter is not easily accessible in a direct way in experiments, we analyze here the generated nonlinear current by the material: this is because the linear current contains a strong response from the incoherent pairs, while the interesting information is contained in the purely nonlinear part. In Fig. 5, we show the 2D current and the corresponding spectra for the (I)–(III), (a) and (b) configurations, indicating the main symmetry contributions to each term, obtained from Fig. 3.

We first notice that the current measured along the x direction [Figs. 5(a)(I), 5(a)(II) and 5(a)(III)] follows the behavior of the gap in Fig. 4, even though the intensity peak for the B_{1g} symmetries (I), (III) is one order of magnitude larger than the one with B_{2g} (II). This can be partly ascribed to the pulse duration and the frequency difference between the quench and the drive, even though the corresponding gap intensities are in the opposite order.

The calculations performed selecting the polarization along the y axis are particularly interesting: In fact, the response of configuration Fig. 5(I)(b) vanishes (in accordance to the symmetry-resolved susceptibility in Fig. 3), and the response in Fig. 5(II)(b) is surprisingly lower than the one in Fig. 5(III)(b), even though the gap for $t = \Delta t$ in the latter case is smaller than in the former. We can also notice that the response in Fig. 5(II)(b) occurs only when quench and drive overlap and extends along the t axis, while the current in Fig. 5(III)(b) is visible only along the diagonal $t = \Delta t$, starting when the driving overlaps with the quench. This means that in the former case the χ_{mdqq}, χ_{mddq} and χ_{mqqd} are the most relevant contributions, while in the latter χ_{mqdd} is, with B_{2g} and B_{1g} dominant symmetry, respectively. Overall, the B_{2g} symmetry is responsible for the gap enhancement from a short pulse, while the B_{1g} symmetry dominates when a long driving is applied, as well as in the nonlinear current generation.

Additional information can be extracted from the 2D spectra, obtained with the Fourier transform of the time-dependent plots (Fig. 6). In general, the signals at $\nu = 0$ are independent of the quench pulse, while all the diagonal lines originate from at least a quench pulse component. The horizontal lines with $\omega = const$, which appear in Fig. 6(I)(a) and Fig. 6(III)(a) in correspondence of the first harmonic signal,
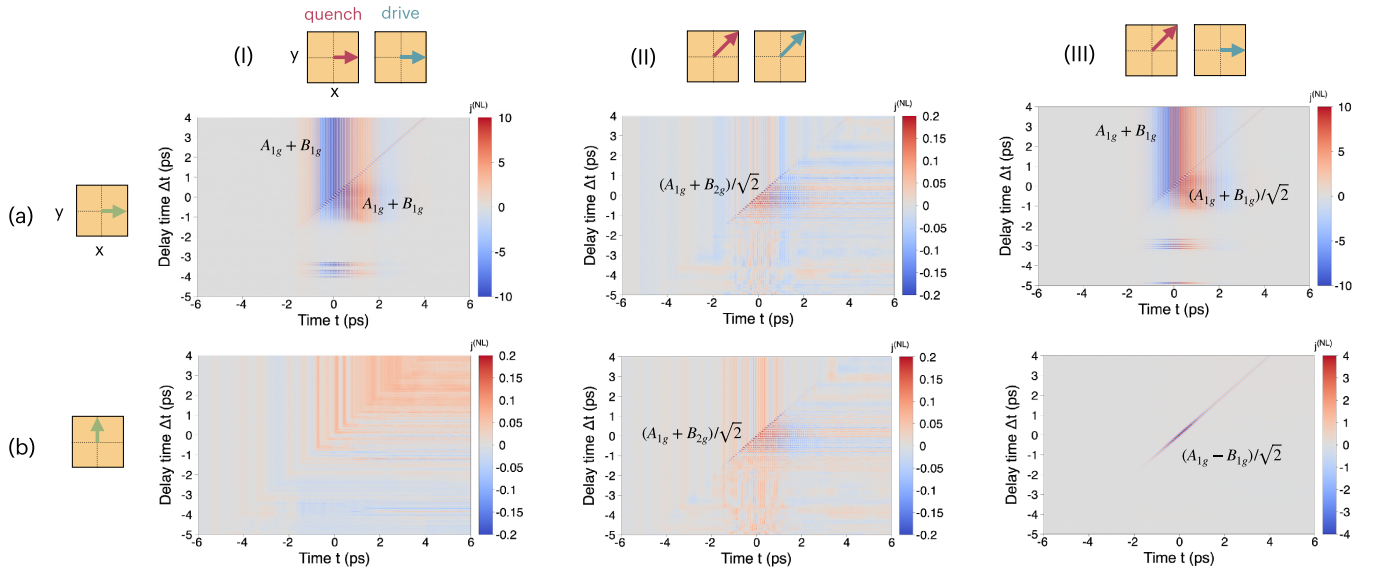
FIG. 5. 2D nonlinear current. Plots of the generated nonlinear current as a function of real time t and the quench-drive delay time Δt for three different schemes (I)–(III) described in the main text, and two polarized output measures along (a) x and (b) y axis, respectively. The symmetries written represent the main contribution according to the table of the nonlinear susceptibilities in Fig. 3. Be aware of the different color scale for each plot.

are also independent on the ω frequency and are generated by $\chi^{(3)}_{mddd}$.

We first notice that, while in the Fig. 6(II)(b) scheme the most prominent features are peaks at ($\omega = \Omega_d$, $\nu = n\Omega_d$) followed by diagonal spectral lines, in Fig. 6(III)(b) the diagonal features peaked below $\omega = \Omega_d$ are more visible, at $\omega \approx \Omega_q$, $\nu \approx \Omega_q$. In particular, the diagonal signal starting from

the origin and with $\omega = -\nu$ is the sum of the contributions of nonlinear susceptibilities $\chi^{(3)}_{mqdd} + \chi^{(3)}_{mddq} + \chi^{(3)}_{mqqq}$.

The third harmonic generated by the driving pulse, appearing along the vertical axis for $\nu = 0$, is generated by the third-order nonlinear susceptibility $\chi^{(3)}_{mddd}$, and appears in Figs. 6(a)(I) and 6(a)(III). Its importance is twofold: First, this generally proves that it is possible to generate a
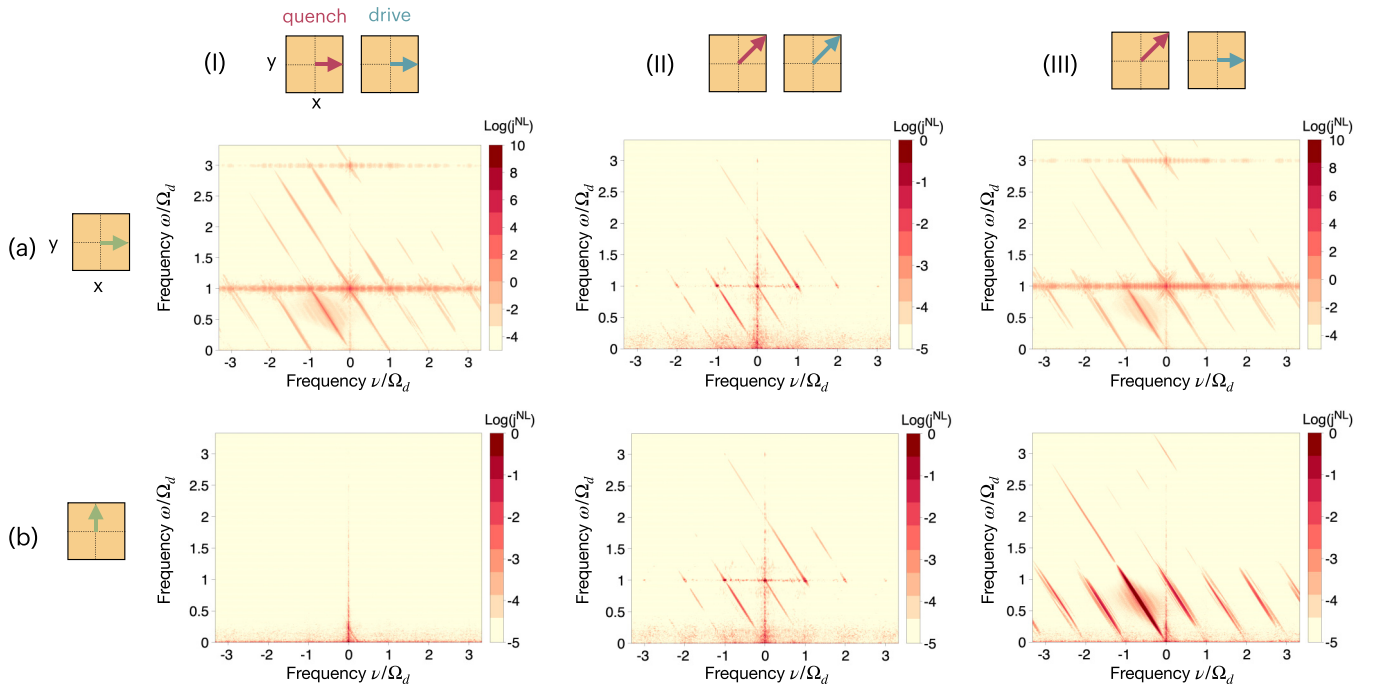

FIG. 6. 2D nonlinear current spectra. Plots of the Fourier transform of the nonlinear current in Fig. 5 for three different schemes (I)–(III) described in the main text, and two polarized output measures along (a) x and (b) y axis, respectively. Be aware of the different log color scale for each plot.

third-harmonic response even in fully incoherent Cooper pairs exhibiting an initially null gap, when properly quenched and driven. This feature has been experimentally shown in cuprate superconductors above their critical temperature, where a phase-fluctuating phase with a vanishing gap is expected [10]. Second, the third harmonic is generated only when the B_{1g} symmetry is explicitly excited (see also Fig. 3). However, we can also notice that in configuration Fig. 6(III)(b) there is a nonvanishing third-harmonic component at $\nu = 0$, originating from a diagonal line which accidentally overlaps with $\nu = 0$ due to a higher-order quench-drive mixing, of the kind $\chi_{mq,qddd}^{(5)}$.

In addition to this analysis, for fully incoherent Cooper pairs, we extended the same approach to partially incoherent superconductors (see Appendix C for the results and a detailed analysis). We have shown that the main features of the symmetry-resolved nonlinear quench-drive spectroscopy are still in place, since they are determined by the symmetry of the underlying Cooper pairing. This would allow us to point whether there are preformed pairs even with a vanishing superconducting order parameter. Moreover, it would be possible to discriminate between a fully incoherent and a partially incoherent superconductor by analyzing the intensity of the third-harmonic signal and especially at its time- and frequency-dependent modulations for given symmetries.

V. CONCLUSION AND OUTLOOK

In this paper, we have calculated the nonlinear response of a phase-fluctuating superconductor with $d_{x^2-y^2}$ pairing symmetry without phase coherence, characterized by vanishing superconducting gap in equilibrium. We have adopted the recently proposed quench-drive spectroscopy scheme [37,38], with THz pulses, inducing a finite superconducting gap and analyzing the generated nonlinear current response. In particular, we have developed a symmetry-resolved analysis, which allows us to selectively address symmetry components according to the quench and drive pulses and the measurement axis chosen.

We have found (i) a nonlinear response even with zero equilibrium order parameter and (ii) induced gap oscillations with predominant B_{1g} and B_{2g} symmetry, according to the spectroscopy scheme. Moreover, (iii) the nonlinear current response has B_{1g} or B_{2g} symmetry according whether it originates from the driving or the quench pulse, respectively, while (iv) the third harmonic generation originates from predominant B_{1g} symmetry excitation. We stress that the results (ii)–(iv) explicitly require the symmetry-based technique introduced in this paper to be obtained, giving one demonstration of the power and relevance of symmetry-resolved quench-drive spectroscopy.

We also highlight that our theoretical approach can be applied to any superconductor and superconducting-related effect, since it is based on the redundancy symmetry breaking to generate a nonlinear response. Moreover, the symmetry-resolved analysis is extremely powerful as it allows us to identify the underlying symmetry of the order parameter, the Cooper pairing, and any physical mechanism giving rise to a photon-induced response. Among these, we mention the possibility to address different collective excitations [30,56], and

even helping in shining light on the superconducting diode effect [57].

APPENDIX A: PSEUDOSPIN MODEL FOR A SUPERCONDUCTOR

In this Appendix, we provide a detailed description of the usage of the pseudospin model to solve the equation of motion of a superconductor when perturbed by an external field. To describe the superconducting phase of a material, we adopt the BCS model expressed by the mean-field Hamiltonian

$$\hat{H}_{\text{BCS}} = \sum_{\mathbf{k},\sigma} \epsilon_{\mathbf{k}} \hat{c}_{\mathbf{k},\sigma}^{\dagger} \hat{c}_{\mathbf{k},\sigma} - \sum_{\mathbf{k}} (\Delta_{\mathbf{k}} \hat{c}_{\mathbf{k},\uparrow}^{\dagger} \hat{c}_{-\mathbf{k},\downarrow}^{\dagger} + \text{H.c.}), \quad (A1)$$

where $\epsilon_{\mathbf{k}} = \xi_{\mathbf{k}} - \mu$, $\xi_{\mathbf{k}}$ is the electronic band dispersion, μ the chemical potential, and $\Delta_{\mathbf{k}}$ the momentum-dependent superconducting order parameter. This latter is described by a complex number which satisfies the gap equation

$$\Delta_{\mathbf{k}} = \sum_{\mathbf{k}'} V_{\mathbf{k},\mathbf{k}'} \langle \hat{c}_{-\mathbf{k}',\downarrow} \hat{c}_{\mathbf{k}',\uparrow} \rangle, \quad (A2)$$

$V_{\mathbf{k},\mathbf{k}'}$ being the (momentum-dependent) pairing interaction. It can be factorized as $V_{\mathbf{k},\mathbf{k}'} = V f_{\mathbf{k}} f_{\mathbf{k}'}$, with $f_{\mathbf{k}} = f_{\mathbf{k}}^{(d_{x^2-y^2})} = (\cos k_x - \cos k_y)/2$ the d-wave form factor of the superconducting order parameter. Therefore, it follows from Eq. (A2) that the gap function itself can be factorized as $\Delta_{\mathbf{k}} = \Delta_0 f_{\mathbf{k}}$.

We now rewrite the BCS Hamiltonian using the pseudospin formalism as [18,53,58]

$$\hat{H}_{\text{BCS}} = \sum_{\mathbf{k}} \mathbf{b}_{\mathbf{k}} \cdot \hat{\sigma}_{\mathbf{k}}, \quad (A3)$$

with the pseudospin vector

$$\hat{\sigma}_{\mathbf{k}} = \frac{1}{2} \hat{\Psi}_{\mathbf{k}}^{\dagger} \tau \hat{\Psi}_{\mathbf{k}}, \quad (A4)$$

which is defined in Nambu-Gor'kov space, with spinor $\hat{\Psi}_{\mathbf{k}}^{\dagger} = (\hat{c}_{\mathbf{k},\uparrow}^{\dagger} \quad \hat{c}_{-\mathbf{k},\downarrow})$ and the Pauli matrices $\tau = (\tau_1, \tau_2, \tau_3)$. The pseudomagnetic field is defined by the vector

$$\mathbf{b}_{\mathbf{k}} = (-2\Delta' f_{\mathbf{k}}, -2\Delta'' f_{\mathbf{k}}, 2\epsilon_{\mathbf{k}}), \quad (A5)$$

where $\epsilon_{\mathbf{k}} = \xi_{\mathbf{k}} - \mu$, $\xi_{\mathbf{k}}$ being the fermionic band dispersion, μ the chemical potential.

In the presence of an external gauge field represented by the vector potential $\mathbf{A}(t)$ coupling to the electrons, the pseudospin changes in time according to

$$\sigma_{\mathbf{k}}(t) = \sigma_{\mathbf{k}}(0) + \delta\sigma_{\mathbf{k}}(t), \quad (A6)$$

with $\delta\sigma_{\mathbf{k}}(t) = (x_{\mathbf{k}}(t), y_{\mathbf{k}}(t), z_{\mathbf{k}}(t))$. The external electromagnetic field is included in the pseudomagnetic field by means of the minimal substitution $\mathbf{k} \rightarrow \mathbf{k} - e\mathbf{A}(t)$ in the fermionic energy, resulting in

$$\mathbf{b}_{\mathbf{k}}(t) = (-2\Delta'(t) f_{\mathbf{k}}, -2\Delta''(t) f_{\mathbf{k}}, \varepsilon_{\mathbf{k}-e\mathbf{A}(t)} + \varepsilon_{\mathbf{k}+e\mathbf{A}(t)}). \quad (A7)$$

The Heisenberg equation of motion for the pseudospin can be written in the Bloch form, $\partial_t \sigma_k = \mathbf{b_k} \times \sigma_{\mathbf{k}}$, providing the set of differential equations

$$
\begin{aligned}
\partial_t x(t) = {} & -(\varepsilon_{\mathbf{k}-e\mathbf{A}} + \varepsilon_{\mathbf{k}+e\mathbf{A}})y(t) - \frac{f_{\mathbf{k}}}{E_{\mathbf{k}}}\epsilon_{\mathbf{k}}\delta\Delta''(t) \\
& + 2\delta\Delta''(t)f_{\mathbf{k}}z(t), \\
\partial_t y(t) = {} & 2\varepsilon_{\mathbf{k}}x(t) + 2(\Delta + \delta\Delta'(t))f_{\mathbf{k}}z(t) \\
& - \delta\Delta' f_{\mathbf{k}}\frac{\epsilon_{\mathbf{k}}}{E_{\mathbf{k}}} + \frac{\Delta f_{\mathbf{k}}}{2E_{\mathbf{k}}}(\varepsilon_{\mathbf{k}-e\mathbf{A}} + \varepsilon_{\mathbf{k}+e\mathbf{A}} - 2\epsilon_{\mathbf{k}}), \\
\partial_t z(t) = {} & -2\,\Delta f_{\mathbf{k}}\,y(t) - \frac{\Delta f_{\mathbf{k}}^2}{E_{\mathbf{k}}}\delta\Delta''(t) - 2\delta\Delta''(t)f_{\mathbf{k}}x(t).
\end{aligned}
$$

(A8)

Here, for simplicity of calculations and without loss of generality, we assumed a real order parameter, $\Delta''(t = 0) = 0$, at the initial time $t = 0$, so $y(0) = 0$.

APPENDIX B: QUENCH-DRIVE NONLINEAR RESPONSE OF A SUPERCONDUCTOR

To describe a quench-drive experiment, we have to choose the appropriate vector potential $\mathbf{A}(t) = \mathbf{A}_q(t) + \mathbf{A}_d(t) = \overline{\mathbf{A}}_q(t - t_q) + \overline{\mathbf{A}}_d(t - t_d)$, where $\mathbf{A}_q(t)$ is the quench pulse centered at time $t = t_q$, $\mathbf{A}_d(t)$ is the driving field centered at $t = t_d$. Introducing the time-delay $\Delta t = t_d - t_q$ and putting $t_d = 0$, we can rewrite $\mathbf{A}(t) = \overline{\mathbf{A}}_q(t + \Delta t) + \overline{\mathbf{A}}_d(\bar{t})$. Therefore, the expressions in Eq. (A8) depend on both t and Δt.

The solution of Eq. (A8) provides the time-dependent pseudospin from which the time-dependent order parameter $\Delta(t)$ and the generated current $j(t)$ can be calculated. From the self-consistent gap equation, we get

$$
\Delta_{\mathbf{k}}(t) = V f_{\mathbf{k}} \sum_{\mathbf{k}'} \sigma_{\mathbf{k}'}^x(t) - i\sigma_{\mathbf{k}'}^y(t). \tag{B1}
$$

The current generated by the superconductor in this quench-drive setup is given by the expression

$$
\mathbf{j}(t, \Delta t) = e \sum_{\mathbf{k}} \mathbf{v}_{\mathbf{k}-e\mathbf{A}(t,\Delta t)}\langle \hat{c}_{\mathbf{k},\uparrow}^\dagger \hat{c}_{\mathbf{k},\uparrow} + \hat{c}_{\mathbf{k},\downarrow}^\dagger \hat{c}_{\mathbf{k},\downarrow}\rangle(t, \Delta t). \tag{B2}
$$

To separate the linear and the nonlinear contributions to the full generated output current, we first expand the velocity in series of powers of the vector potential $\mathbf{A}$:

$$
\mathbf{v}_{\mathbf{k}-e\mathbf{A}(t,\Delta t)} = \mathbf{v}_{\mathbf{k}} + \nabla_{\mathbf{A}}(\mathbf{v}_{\mathbf{k}-e\mathbf{A}(t,\Delta t)})|_{\mathbf{A}=\mathbf{0}} \cdot \mathbf{A} + \dots. \tag{B3}
$$

We note that $\nabla_{\mathbf{A}}(\cdot)|_{\mathbf{A}=\mathbf{0}} = [\nabla_{\mathbf{A}}(\kappa) \quad \nabla_\kappa(\cdot)]|_{\mathbf{A}=\mathbf{0}} = -e \, \nabla_\kappa(\cdot)|_{\mathbf{A}=\mathbf{0}}$, with $\kappa = \mathbf{k} - e\mathbf{A}$. Here we omitted the explicit time dependence of $\mathbf{A}$ and κ from t and Δt. Now we can rewrite Eq. (B3) as

$$
\mathbf{v}_\kappa = \mathbf{v}_{\mathbf{k}} - e \, \nabla_\kappa \mathbf{v}_\kappa|_{\mathbf{A}=\mathbf{0}} \cdot \mathbf{A} + \dots. \tag{B4}
$$

In particular, the equivalence $\nabla_\kappa \mathbf{v}_\kappa|_{\mathbf{A}=\mathbf{0}} = \nabla_{\mathbf{k}}\mathbf{v}_{\mathbf{k}}$ holds. Therefore, we can simplify Eq. (B3) writing

$$
\mathbf{v}_{\mathbf{k}} = \mathbf{v}_{\mathbf{k}} - e\,\mathbf{A}\cdot\nabla_{\mathbf{k}}\mathbf{v}_{\mathbf{k}} + \dots. \tag{B5}
$$

Additionally, we expand the electron number

$$
\langle \hat{n}_{\mathbf{k}}\rangle(t, \Delta t) = 2z_{\mathbf{k}}(t, \Delta t) + 2\hat{\sigma}_{\mathbf{k}}^z(0) + 1, \tag{B6}
$$

where we used the relation $\hat{n}_{\mathbf{k}} = 2\hat{\sigma}_{\mathbf{k}}^z + 1$. Therefore, Eq. (B2) can be expanded in the lowest orders as

$$
\begin{aligned}
\mathbf{j}(t, \Delta t) \approx {} & e \sum_{\mathbf{k}} (\mathbf{v}_{\mathbf{k}} - e\,\mathbf{A}(t, \Delta t)\cdot\nabla_{\mathbf{k}}\mathbf{v}_{\mathbf{k}}) \\
& \cdot \left(2z_{\mathbf{k}}(t, \Delta t) + 2\hat{\sigma}_{\mathbf{k}}^z(0) + 1\right).
\end{aligned} \tag{B7}
$$

We can decompose the generated current along a generic x' axis to extract specific symmetry components:

$$
\begin{aligned}
\mathbf{j}_{x'}(t, \Delta t) & = (\mathbf{j}(t, \Delta t)\cdot\hat{x}')\,\hat{x}' \\
& = (j_x(t, \Delta t)\cos\theta + j_y(t, \Delta t)\sin\theta)\,\hat{x}'.
\end{aligned} \tag{B8}
$$

The contribution to the current in Eq. (B7) at the lowest order in the external field is given by

$$
\mathbf{j}^{(0)}(t, \Delta t) = e \sum_{\mathbf{k}} \mathbf{v}_{\mathbf{k}}\left(2\hat{\sigma}_{\mathbf{k}}^z(t, \Delta t) + 1\right), \tag{B9}
$$

which vanishes due to parity. At the next order, the linear term reads

$$
\mathbf{j}^{(1)}(t, \Delta t) = -e^2 \sum_{\mathbf{k}} \mathbf{A}(t, \Delta t)\cdot\nabla_{\mathbf{k}}\mathbf{v}_{\mathbf{k}}\left(2\hat{\sigma}_{\mathbf{k}}^z(0) + 1\right). \tag{B10}
$$

The full nonlinear response, which is given by the sum of all the odd orders of the current expansion, can be conveniently calculated by

$$
\mathbf{j}^{(NL)}(t, \Delta t) = e \sum_{\mathbf{k}} \mathbf{v}_{\mathbf{k}-e\mathbf{A}(t,\Delta t)}\left(2\hat{\sigma}_{\mathbf{k}}^z(t, \Delta t) - 2\hat{\sigma}_{\mathbf{k}}^z(0)\right). \tag{B11}
$$

We can also explicitly write the expression of the dominant nonvanishing nonlinear term generated by the driving pulse, the third order component, as follows:

$$
\mathbf{j}^{(3)}(t, \Delta t) = -2e^2 \sum_{\mathbf{k}} z_{\mathbf{k}}(t, \Delta t)\,\mathbf{A}(t, \Delta t)\cdot\nabla_{\mathbf{k}}\mathbf{v}_{\mathbf{k}}, \tag{B12}
$$

where $z_{\mathbf{k}}(t, \Delta t)$ is the third component of the pseudospin vector $\sigma_{\mathbf{k}}(t, \Delta t)$, containing the information of the state of the system perturbed by the quench pulse. The paramagnetic term is neglected here due to suppression by parity [18].

In general, it is useful to extract the 2D frequency spectrum of such a response to analyze the relevant high harmonics: For this reason, we compute the 2D Fourier transform with respect to the evolution time t and the quench-drive delay time Δt, obtaining the reciprocal variables $\omega \equiv \tilde{\mathcal{F}}(t)$ and $\nu \equiv \tilde{\mathcal{F}}(\Delta t)$, respectively.

As an example, the 2D Fourier transform of Eq. (B12) to provide the third-harmonic response of the driving frequency along the direction $\hat{x}'$ is

$$
\begin{aligned}
j_{x'}^{(3)}(\omega = 3\Omega_d, \nu) = {} & -2e^2 A_d \sum_{\mathbf{k}} F_{x'}(\mathbf{k})\,z_{\mathbf{k}}(\omega = 2\Omega_d, \nu) \\
& -2e^2 A_d \sum_{\mathbf{k}} F_{x'}(\mathbf{k})\,z_{\mathbf{k}}(\omega = 4\Omega_d, \nu),
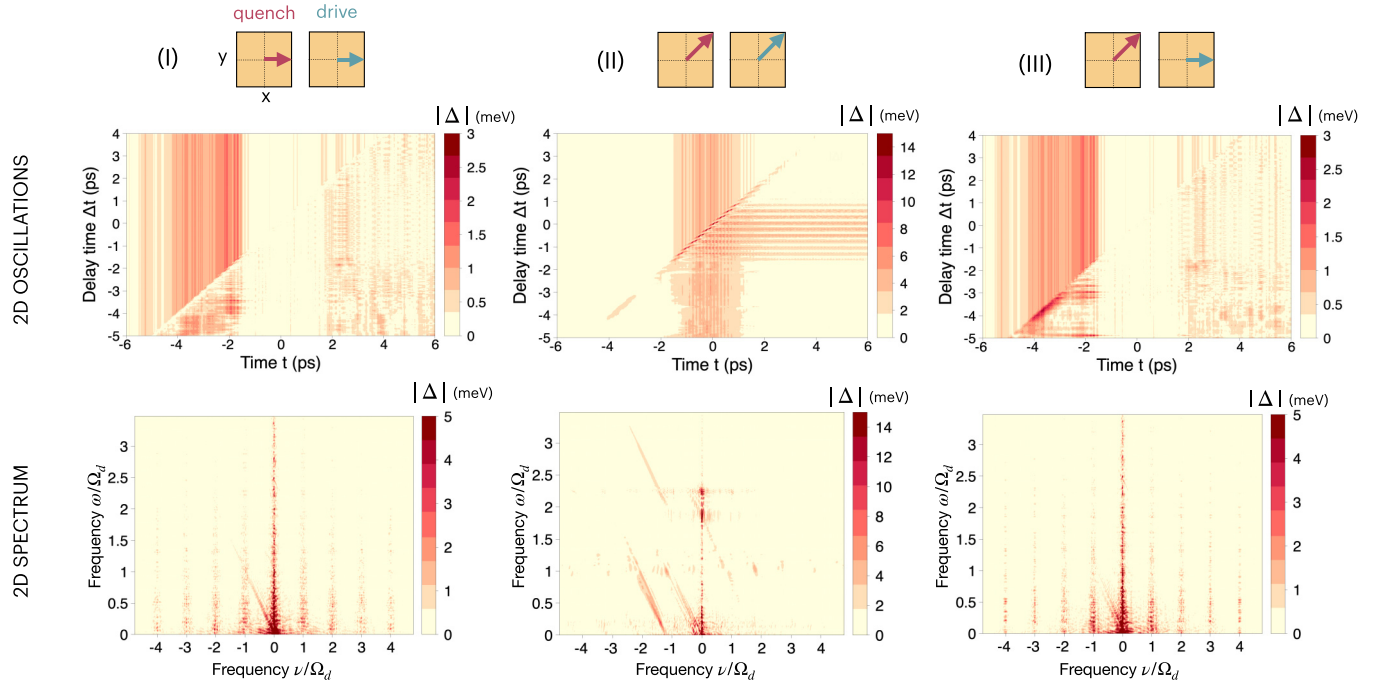\end{aligned} \tag{B13}
$$

FIG. 7. Gap oscillations and frequency spectra. (a) 2D oscillations in $(t, \Delta t)$ of the absolute value of the superconducting gap, $|\Delta|$, for the three scheme configurations (I)–(III) described in the main text and illustrated by the plots of quench and drive pulses. (b) Absolute value of the 2D Fourier transform of the full complex gap, $|\mathcal{F}\{\Delta(t, \Delta t)\}| = |\Delta(\omega, \nu)|$.

where $F_{x'}$ is an appropriate function independent of the frequency which contains information on the driving shape, the measurement axis, and the quasiparticles' momentum.

APPENDIX C: ADDITIONAL RESULTS

We present here additional results, obtained for the same quench and drive intensities as the ones in the main text, i.e., $A_d = A_q = 0.8$, as well as the pulses' duration and shape, but with different frequencies, namely, $\Omega_d = 3.66$ THz and $\Omega_q = 7.48$ THz, respectively. As a consequence, the quench is nearly resonant with the maximum superconducting equilibrium gap, $\Delta_{\max} = 31$ meV $= 7.5$ THz, while the driving pulse is far from it. The generated nonlinear current is therefore affected by these conditions, and the response appears in some cases qualitatively and quantitatively different from the one obtained in the main text, even if the symmetries involved in the quench-drive spectra are the same.

We first analyze the behavior of the absolute value of the superconducting gap as a function of the real time t and the delay time Δt. Interestingly, we realize that the gap is very poorly excited in configurations (I) and (III) due to the B_{1g} symmetry and the driving contribution, with a maximum amplitude of about 3 meV, and as low as 1 meV on the central peak of the driving field at $t = 0$. On the other hand, scheme (II) has a higher gap excitation. The corresponding 2D Fourier spectra show that, for schemes (I) and (III) there are no proper gap oscillations, but rather an almost frequency-independent enhancement, plus quench-induced contributions [vertical lines in Figs. 7(I) and 7(III)(b)]. On the other hand, for scheme (II) with diagonal quench and drive pulses, where the B_{2g} symmetry is excited, a gap oscillation at $\omega = 2\Omega_d$ due to the driving appears, as well as at $\omega = 2\Delta$, which includes

Higgs and quasiparticles' excitations at twice the induced gap amplitude, around 8.5 meV.

We now turn to the generated current: Due to the different resonance conditions, we expect the current responses involving a quench pulse to be more intense, saturating the purely drive signals. In particular, for schemes (I) and (III) where the gap excitation and oscillations are much smaller, we expect the susceptibility term independent of the frequency to be the most relevant [8].

In Figs. 8 and 9, the measured nonlinear responses in time and the corresponding 2D Fourier spectra are shown, respectively. We notice that the current measured along the x axis for schemes (I) and (III), involving mainly the B_{1g} symmetry, is quantitatively different from the one in Fig. 5. The lower intensity (the scales of Figs. 5 and 8 are different), in fact, is explained by the fact that the main response involves the driving pulse, and the corresponding susceptibility is now more far from resonance. On the other hand, scheme (II), with quench and drive pulses along the $\hat{x}\hat{y}$ diagonal axis, now provides a slightly stronger response, involving mainly the quench pulse.

The 2D Fourier spectra in Fig. 9 are even more dense of information. In fact, the spectra of schemes (I) and (III) present much fewer features than with the choices of frequency in the main text: in particular, Figs. 9(I)(a) and 9(II)(a) have a weaker third harmonic generation and only one diagonal line, representing the nonequilibrium modulation due to the quench pulses. Moreover, the current measured along the y axis in Fig. 9(III)(b) has no first harmonic contribution, and is saturated by the same nonequilibrium modulation of Fig. 9(I),(III)(a). On the other hand, the spectra of Figs. 9(a)(II) and 9(b)(II) are much more complex, exhibiting more and stronger frequency
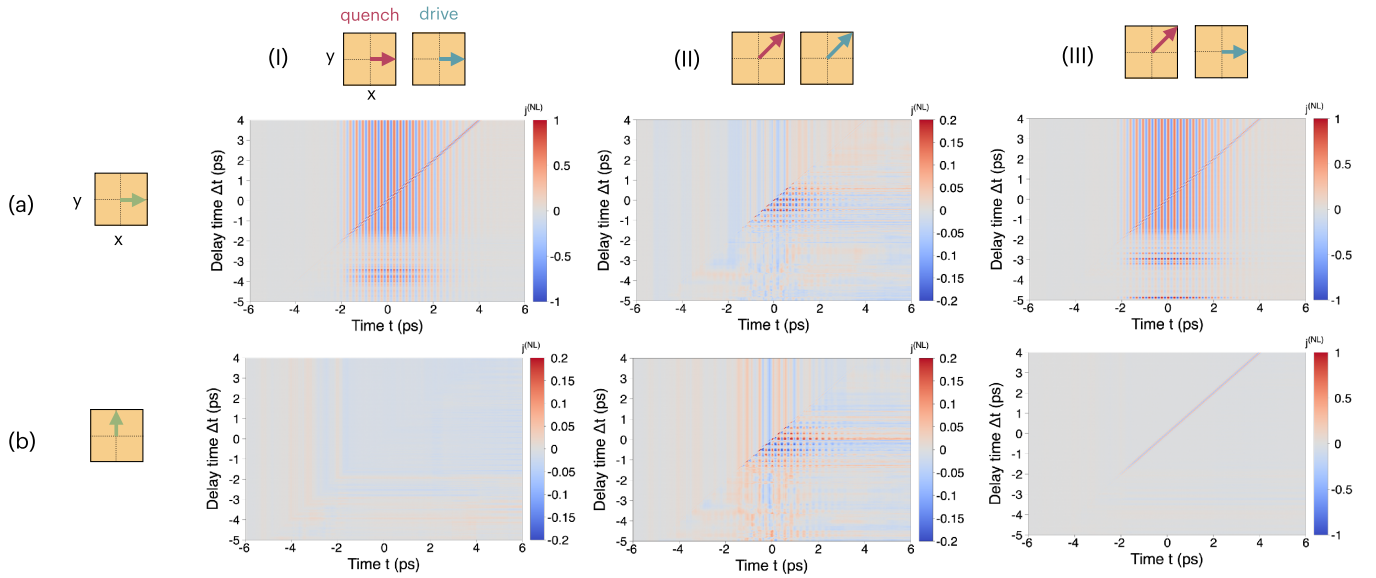
FIG. 8. 2D nonlinear current. Plots of the generated nonlinear current as a function of real time t and the quench-drive delay time Δt for three different schemes (I)–(III) described in the main text and two polarized output measures along (a) x and (b) y axis, respectively. This figure corresponds to Fig. 5, here obtained with different frequencies of quench and drive pulses, as explained in the main text. Be aware of the different color scale for each plot and with respect to Fig. 5.

modulations and the emergence of a nonequilibrium third harmonic at $\omega = 3\Omega_d$, $\nu = 0$.

All in all, we have observed how the nonlinear signal is still present in (I) and (III) configurations, the current intensity being higher than in scheme (II), even if the gap is less excited in the former. The reason of this behavior can be ascribed once again to the symmetries involved and here identified.

We now turn to consider a phase-fluctuating superconductor with $\phi_{\max} = \pi/8$. In this situation, the superconducting order parameter is nonzero even in equilibrium, and the resonance energy of the quasiparticles' fluctuations is much higher. We present in Figs. 10 and 11 the symmetry-resolved 2D nonlinear current and the corresponding Fourier transform signals in frequency, respectively. As we can notice, these
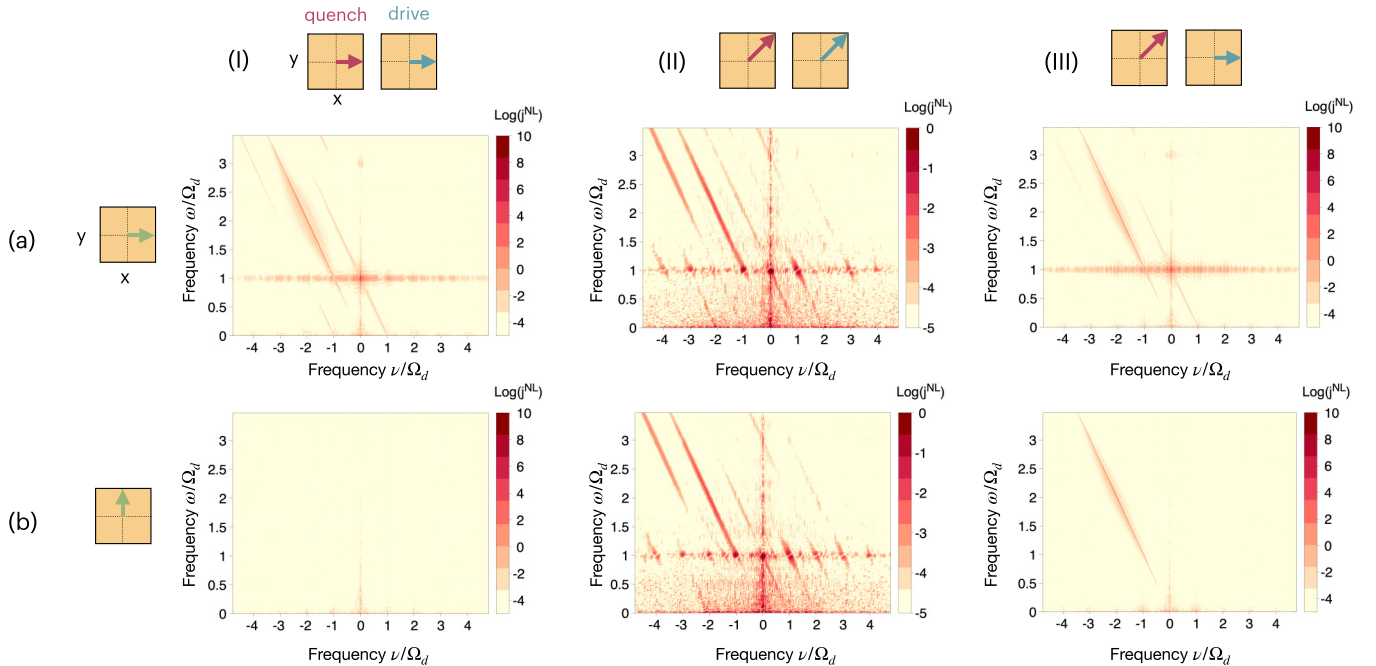

FIG. 9. 2D nonlinear current spectra. Plots of the Fourier transform of the nonlinear current in Fig. 8 for three different schemes (I)-(III) described in the main text and two polarized output measures along (a) x and (b) y axis, respectively. This figure corresponds to Fig. 6, here obtained with different frequencies of quench and drive pulses, as explained in the main text. Be aware of the different log color scale for each plot.
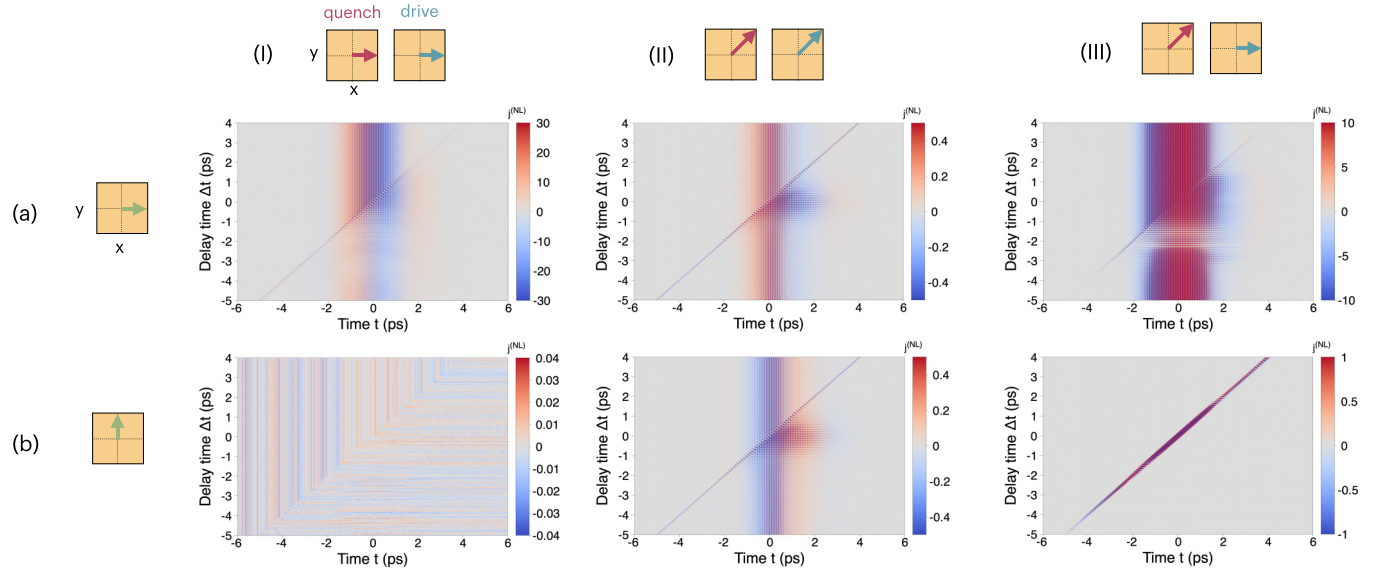
FIG. 10. 2D nonlinear current for partially incoherent pairs. Plots of the generated nonlinear current as a function of real time t and the quench-drive delay time Δt for three different schemes (I)–(III) described in the main text, and two polarized output measures along (a) x and (b) y axis, respectively. This figure corresponds to Fig. 5, here obtained for phase-fluctuating superconductors with $\phi_{max} = \pi/8$. Be aware of the different color scale for each plot and with respect to Fig. 5.

are qualitatively similar to the results of Figs. 5 and 6: this demonstrates that the nonlinear current response originates mainly from the presence of the underlying Cooper pairing, which allows us to transiently enhance the superconducting gap in the quench-drive setup. However, we notice here significant quantitative differences with respect to the purely incoherent case. In fact, it is possible to notice in Fig. 10

the higher intensity in all the nonvanishing responses. Interestingly, this quantitative aspect leads to a non-negligible qualitative difference: namely, the third harmonic signal for configurations Figs. 11(a)(II) and 11(b)(II) is quantitatively distinguishable, and the ones in Figs. 11(a)(I) and 11(a)(III) have numerous features which modulate its time evolution with frequencies multiple of the driving frequency Ω_d. In
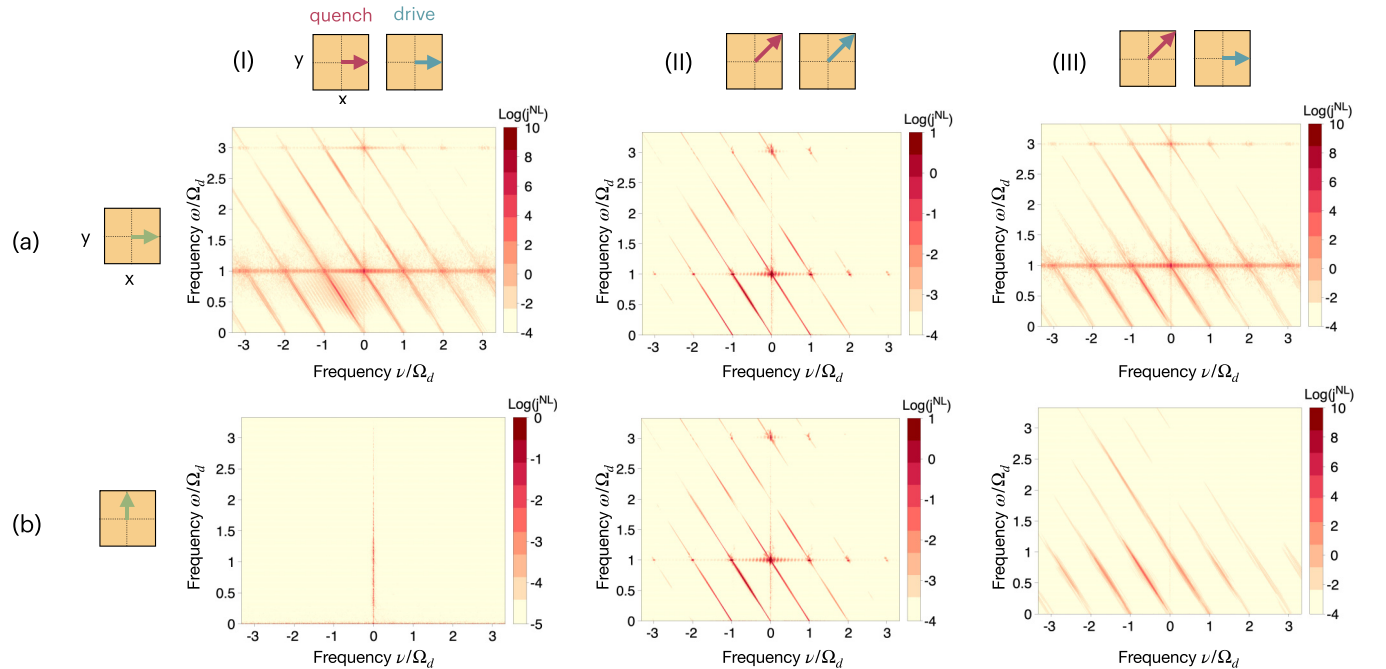

FIG. 11. 2D nonlinear current spectra for partially incoherent pairs. Plots of the Fourier transform of the nonlinear current in Fig. 8 for three different schemes (I)–(III) described in the main text and two polarized output measures along (a) x and (b) y axis, respectively. This figure corresponds to Fig. 6, here obtained for phase-fluctuating superconductors with $\phi_{max} = \pi/8$. Be aware of the different log color scale for each plot.

conclusion, we can claim that the main features of the symmetry-resolved nonlinear quench-drive spectroscopy are determined by the symmetry of the underlying Cooper pairing, allowing us to distinguish whether there are preformed pairs even the in absence of a superconducting order param-

eter. However, it would be possible to discriminate between a fully incoherent and a partially incoherent superconductor by analyzing the intensity of the third-harmonic signal and especially at its time- and frequency-dependent modulations for given symmetries.

---

[1] M. K. Wu, J. R. Ashburn, C. J. Torng, P. H. Hor, R. L. Meng, L. Gao, Z. J. Huang, Y. Q. Wang, and C. W. Chu, Superconductivity at 93 K in a new mixed-phase Y-Ba-Cu-O compound system at ambient pressure, Phys. Rev. Lett. **58**, 908 (1987).

[2] H. Maeda, Y. Tanaka, M. Fukutomi, and T. Asano, A new high-T_c oxide superconductor without a rare earth element, Jpn. J. Appl. Phys. **27**, L209 (1988).

[3] B. Keimer, S. A. Kivelson, M. R. Norman, S. Uchida, and J. Zaanen, From quantum matter to high-temperature superconductivity in copper oxides, Nature (London) **518**, 179 (2015).

[4] Y. Toda, F. Kawanokami, T. Kurosawa, M. Oda, I. Madan, T. Mertelj, V. V. Kabanov, and D. Mihailovic, Rotational symmetry breaking in $Bi_2Sr_2CaCu_2O_{8+\delta}$ probed by polarized femtosecond spectroscopy, Phys. Rev. B **90**, 094513 (2014).

[5] T. P. Devereaux, D. Einzel, B. Stadlober, R. Hackl, D. H. Leach, and J. J. Neumeier, Electronic Raman scattering in high-T_c superconductors: A probe of $d_{x^2-y^2}$ pairing, Phys. Rev. Lett. **72**, 396 (1994).

[6] R. S. Markiewicz, S. Sahrakorpi, M. Lindroos, H. Lin, and A. Bansil, One-band tight-binding model parametrization of the high-T_c cuprates including the effect of k_z dispersion, Phys. Rev. B **72**, 054519 (2005).

[7] R. Matsunaga, N. Tsuji, H. Fujita, A. Sugioka, K. Makise, Y. Uzawa, H. Terai, Z. Wang, H. Aoki, and R. Shimano, Light-induced collective pseudospin precession resonating with Higgs mode in a superconductor, Science **345**, 1145 (2014).

[8] T. Cea, C. Castellani, and L. Benfatto, Nonlinear optical effects and third-harmonic generation in superconductors: Cooper pairs versus Higgs mode contribution, Phys. Rev. B **93**, 180507(R) (2016).

[9] K. Katsumi, N. Tsuji, Y. I. Hamada, R. Matsunaga, J. Schneeloch, R. D. Zhong, G. D. Gu, H. Aoki, Y. Gallais, and R. Shimano, Higgs mode in the d-wave superconductor $Bi_2Sr_2CaCu_2O_{8+x}$ driven by an intense terahertz pulse, Phys. Rev. Lett. **120**, 117001 (2018).

[10] H. Chu, M.-J. Kim, K. Katsumi, S. Kovalev, R. D. Dawson, L. Schwarz, N. Yoshikawa, G. Kim, D. Putzky, Z. Z. Li *et al.*, Phase-resolved Higgs response in superconducting cuprates, Nat. Commun. **11**, 1793 (2020).

[11] M. Puviani, A. Baum, S. Ono, Y. Ando, R. Hackl, and D. Manske, Calculation of an enhanced A_{1g} symmetry mode induced by Higgs oscillations in the Raman spectrum of high-temperature cuprate superconductors, Phys. Rev. Lett. **127**, 197001 (2021).

[12] H. Chu, S. Kovalev, Z. X. Wang, L. Schwarz, T. Dong, L. Feng, R. Haenel, M.-J. Kim, P. Shabestari, H. L. Phuong, K. Honasoge, R. D. Dawson, D. Putzky, G. Kim, M. Puviani, M. Chen, N. Awari, A. N. Ponomaryov, I. Ilyakov, M. Bluschke *et al.*, Fano interference of the Higgs mode in cuprate high-T_c superconductors, Nat. Commun. **14**, 1343 (2023).

[13] T. E. Glier, M. Rerrer, L. Westphal, G. Lüllau, L. Feng, S. Tian, R. Haenel, M. Zonno, H. Eisaki, M. Greven, A. Damascelli, S. Kaiser, D. Manske, and M. Rübhausen, Direct observation of the Higgs mode in a superconductor by non-equilibrium Raman scattering, arXiv:2310.08162.

[14] B. Cheng, D. Cheng, K. Lee, M. Mootz, C. Huang, L. Luo, Z. Chen, Y. Lee, B. Y. Wang, I. E. Perakis, Z.-X. Shen, H. Y. Hwang, and J. Wang, Evidence for highly damped Higgs mode in infinite-layer nickelates, arXiv:2310.02589.

[15] J. M. Harris, Z. X. Shen, P. J. White, D. S. Marshall, M. C. Schabel, J. N. Eckstein, and I. Bozovic, Anomalous superconducting state gap size versus T_c behavior in underdoped $Bi_2Sr_2Ca_{1-x}Dy_xCu_2O_{8+\delta}$, Phys. Rev. B **54**, R15665(R) (1996).

[16] Y. Wang, L. Li, M. J. Naughton, G. D. Gu, S. Uchida, and N. P. Ong, Field-enhanced diamagnetism in the pseudogap state of the cuprate $Bi_2Sr_2CaCu_2O_{8+\delta}$ superconductor in an intense magnetic field, Phys. Rev. Lett. **95**, 247002 (2005).

[17] P. M. C. Rourke, I. Mouzopoulou, X. Xu, C. Panagopoulos, Y. Wang, B. Vignolle, C. Proust, E. V. Kurganova, U. Zeitler, Y. Tanabe, T. Adachi, Y. Koike, and N. E. Hussey, Phase-fluctuating superconductivity in overdoped $La_{2-x}Sr_xCuO4$, Nat. Phys. **7**, 455 (2011).

[18] L. Schwarz and D. Manske, Theory of driven Higgs oscillations and third-harmonic generation in unconventional superconductors, Phys. Rev. B **101**, 184519 (2020).

[19] T. Cea, P. Barone, C. Castellani, and L. Benfatto, Polarization dependence of the third-harmonic generation in multiband superconductors, Phys. Rev. B **97**, 094516 (2018).

[20] L. Schwarz, B. Fauseweh, N. Tsuji, N. Cheng, N. Bittner, H. Krull, M. Berciu, G. S. Uhrig, A. P. Schnyder, S. Kaiser, and D. Manske, Classification and characterization of nonequilibrium Higgs modes in unconventional superconductors, Nat. Commun. **11**, 287 (2020).

[21] M. Udina, J. Fiore, T. Cea, C. Castellani, G. Seibold, and L. Benfatto, THz non-linear optical response in cuprates: Predominance of the BCS response over the Higgs mode, Faraday Discuss. **237**, 168 (2022).

[22] M. Alías-Rodríguez, M. Basini, L. Benfatto, Y. Boeije, I. Burghardt, A. Burnett, L. Chen, E. Collet, R. Cowin, I. Eremin, G. Fleming, A. V. Girija, K. Ishida, S. Iwai, J. O. Johansson, S. L. Johnson, K. Katsumi, J. McCusker, C. Odin, M. Puviani *et al.*, Theory of out of equilibrium light-induced phenomena: General discussion, Faraday Discuss. **237**, 198 (2022).

[23] K. Katsumi, J. Fiore, M. Udina, R. R. I. au2, D. Barbalas, J. Jesudasan, P. Raychaudhuri, G. Seibold, L. Benfatto, and N. P. Armitage, Revealing novel aspects of light-matter coupling in terahertz two-dimensional coherent spectroscopy: The case of the amplitude mode in superconductors, arXiv:2311.16449.

[24] F. Giusti, A. Marciniak, F. Randi, G. Sparapassi, F. Boschini, H. Eisaki, M. Greven, A. Damascelli, A. Avella, and D. Fausti, Signatures of enhanced superconducting phase coherence in optimally doped $Bi_2Sr_2Y_{0.08}Ca_{0.92}Cu_2O_{8+\delta}$ driven

by midinfrared pulse excitations, Phys. Rev. Lett. **122**, 067002 (2019).

[25] V. J. Emery and S. A. Kivelson, Importance of phase fluctuations in superconductors with small superfluid density, Nature (London) **374**, 434 (1995).

[26] J. Corson, R. Mallozzi, J. Orenstein, J. N. Eckstein, and I. Bozovic, Vanishing of phase coherence in underdoped $Bi_2Sr_2CaCu_2O_{8+\delta}$, Nature (London) **398**, 221 (1999).

[27] Z. A. Xu, N. P. Ong, Y. Wang, T. Kakeshita, and S. Uchida, Vortex-like excitations and the onset of superconducting phase fluctuation in underdoped $La_{2-x}Sr_xCuO4$, Nature (London) **406**, 486 (2000).

[28] F. Giusti, A. Montanaro, A. Marciniak, F. Randi, F. Boschini, F. Glerean, G. Jarc, H. Eisaki, M. Greven, A. Damascelli, A. Avella, and D. Fausti, Anisotropic time-domain electronic response in cuprates driven by midinfrared pulses, Phys. Rev. B **104**, 125121 (2021).

[29] M. Buzzi, G. Jotzu, A. Cavalleri, J. I. Cirac, E. A. Demler, B. I. Halperin, M. D. Lukin, T. Shi, Y. Wang, and D. Podolsky, Higgs-mediated optical amplification in a nonequilibrium superconductor, Phys. Rev. X **11**, 011055 (2021).

[30] M. Udina, T. Cea, and L. Benfatto, Theory of coherent-oscillations generation in terahertz pump-probe spectroscopy: From phonons to electronic collective modes, Phys. Rev. B **100**, 165131 (2019).

[31] F. Giorgianni, T. Cea, C. Vicario, C. P. Hauri, W. K. Withanage, X. Xi, and L. Benfatto, Leggett mode controlled by light pulses, Nat. Phys. **15**, 341 (2019).

[32] S. T. Cundiff and S. Mukamel, Optical multidimensional coherent spectroscopy, Phys. Today **66**(7), 44 (2013).

[33] M. Woerner, W. Kuehn, P. Bowlan, K. Reimann, and T. Elsaesser, Ultrafast two-dimensional terahertz spectroscopy of elementary excitations in solids, New J. Phys. **15**, 025039 (2013).

[34] J. Lu, X. Li, H. Y. Hwang, B. K. Ofori-Okai, T. Kurihara, T. Suemoto, and K. A. Nelson, Coherent two-dimensional terahertz magnetic resonance spectroscopy of collective spin waves, Phys. Rev. Lett. **118**, 207204 (2017).

[35] Y. Wan and N. P. Armitage, Resolving continua of fractional excitations by spinon echo in THz 2D coherent spectroscopy, Phys. Rev. Lett. **122**, 257401 (2019).

[36] F. Mahmood, D. Chaudhuri, S. Gopalakrishnan, R. Nandkishore, and N. P. Armitage, Observation of a marginal Fermi glass, Nat. Phys. **17**, 627 (2021).

[37] M. Puviani and D. Manske, Quench-drive spectroscopy of cuprates, Faraday Discuss. **237**, 125 (2022).

[38] M. Puviani, R. Haenel, and D. Manske, Quench-drive spectroscopy and high-harmonic generation in BCS superconductors, Phys. Rev. B **107**, 094501 (2023).

[39] M.-J. Kim, S. Kovalev, M. Udina, R. Haenel, G. Kim, M. Puviani, G. Cristiani, I. Ilyakov, T. V. A. G. de Oliveira, A. Ponomaryov, J.-C. Deinert, G. Logvenov, B. Keimer, D. Manske, L. Benfatto, and S. Kaiser, Tracing the dynamics of superconducting order via transient third harmonic generation, Sci. Adv. **10**, eadi7598 (2024).

[40] M. Mootz, L. Luo, J. Wang, and l. E. Perakis, Visualization and quantum control of light-accelerated condensates by terahertz multi-dimensional coherent spectroscopy, Commun. Phys. **5**, 47 (2022).

[41] L. Luo, M. Mootz, J. H. Kang, C. Huang, K. Eom, J. W. Lee, C. Vaswani, Y. G. Collantes, E. E. Hellstrom, I. E. Perakis, C. B. Eom, and J. Wang, Quantum coherence tomography of light-controlled superconductivity, Nat. Phys. **19**, 201 (2023).

[42] M. Mootz, P. P. Orth, C. Huang, L. Luo, J. Wang, and Y.-X. Yao, Two-dimensional coherent spectrum of high-spin models via a quantum computing approach, Quantum Sci. Technol. (to be published).

[43] M. Mootz, L. Luo, C. Huang, J. Wang, and llias E. Perakis, Multi-dimensional coherent spectroscopy of light-driven states and their collective modes in multi-band superconductors, Phys. Rev. B **109**, 014515 (2024).

[44] A. G. Salvador, P. E. Dolgirev, M. H. Michael, A. Liu, D. Pavicevic, M. Fechner, A. Cavalleri, and E. Demler, Principles of 2D terahertz spectroscopy of collective excitations: The case of Josephson plasmons in layered superconductors, arXiv:2401.05503.

[45] T. P. Devereaux and D. Einzel, Electronic Raman scattering in superconductors as a probe of anisotropic electron pairing, Phys. Rev. B **51**, 16336 (1995).

[46] T. P. Devereaux and R. Hackl, Inelastic light scattering from correlated electrons, Rev. Mod. Phys. **79**, 175 (2007).

[47] T. Kondo, W. Malaeb, Y. Ishida, T. Sasagawa, H. Sakamoto, T. Takeuchi, T. Tohyama, and S. Shin, Point nodes persisting far beyond T_c in Bi2212, Nat. Commun. **6**, 7699 (2015).

[48] I. Madan, T. Kurosawa, Y. Toda, M. Oda, T. Mertelj, P. Kusar, and D. Mihailovic, Separating pairing from quantum phase coherence dynamics above the superconducting transition by femtosecond spectroscopy, Sci. Rep. **4**, 5656 (2014).

[49] T. J. Reber, N. C. Plumb, Y. Cao, Z. Sun, Q. Wang, K. McElroy, H. Iwasawa, M. Arita, J. S. Wen, Z. J. Xu, G. Gu, Y. Yoshida, H. Eisaki, Y. Aiura, and D. S. Dessau, Prepairing and the "filling" gap in the cuprates from the tomographic density of states, Phys. Rev. B **87**, 060506(R) (2013).

[50] G. Yu, D.-D. Xia, D. Pelc, R.-H. He, N.-H. Kaneko, T. Sasagawa, Y. Li, X. Zhao, N. Barišić, A. Shekhter, and M. Greven, Universal precursor of superconductivity in the cuprates, Phys. Rev. B **99**, 214502 (2019).

[51] D. Pelc, M. Vučković, M. S. Grbić, M. Požek, G. Yu, T. Sasagawa, M. Greven, and N. Barišić, Emergence of superconductivity in the cuprates via a universal percolation process, Nat. Commun. **9**, 4327 (2018).

[52] P. Popčević, D. Pelc, Y. Tang, K. Velebit, Z. Anderson, V. Nagarajan, G. Yu, M. Požek, N. Barišić, and M. Greven, Percolative nature of the direct-current paraconductivity in cuprate superconductors, npj Quantum Mater. **3**, 42 (2018).

[53] P. W. Anderson, Random-phase approximation in the theory of superconductivity, Phys. Rev. **112**, 1900 (1958).

[54] A. Ghatak and T. Das, Theory of superconductivity with non-Hermitian and parity-time reversal symmetric Cooper pairing symmetry, Phys. Rev. B **97**, 014512 (2018).

[55] R. Matsunaga, N. Tsuji, K. Makise, H. Terai, H. Aoki, and R. Shimano, Polarization-resolved terahertz third-harmonic generation in a single-crystal superconductor NbN: Dominance of the

Higgs mode beyond the BCS approximation, Phys. Rev. B **96**, 020505(R) (2017).

[56] F. Gabriele, M. Udina, and L. Benfatto, Non-linear terahertz driving of plasma waves in layered cuprates, Nat. Commun. **12**, 752 (2021).

[57] M. Nadeem, M. S. Fuhrer, and X. Wang, The superconducting diode effect, Nat. Rev. Phys. **5**, 558 (2023).

[58] N. Tsuji and H. Aoki, Theory of Anderson pseudospin resonance with Higgs mode in superconductors, Phys. Rev. B **92**, 064508 (2015).